Nanoscale

Accepted Manuscript

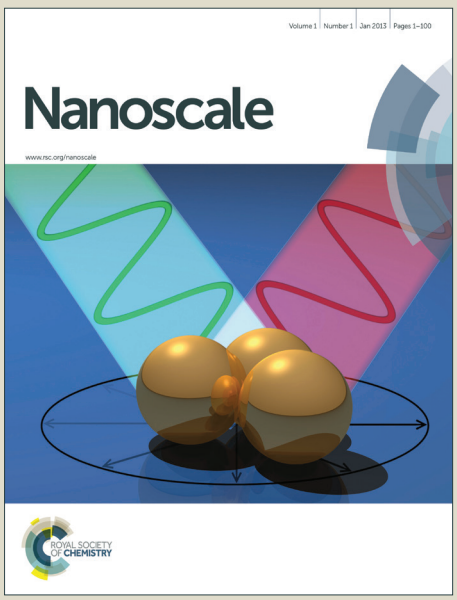

ROYAL SOCIETY OF CHEMISTRY

www.rsc.org/nanoscale

Journal Name

RSCPublishing

ARTICLE

NGF-conjugated Iron Oxide Nanoparticles promote differentiation and outgrowth of PC12 cells

Cite this: DOI: 10.1039/xoxxoooooox

M. Marcus,[a,c] H. Skaat,[b,c] N. Alon, [a,c] S. Margel[b,c] and O. Shefi*[a,c]

Received ooth January 2012,
Accepted ooth January 2012

DOI: 10.1039/xoxxoooooox

www.rsc.org/

The search for regenerative agents that promote neuronal differentiation and repair is of great importance. Nerve growth factor (NGF) which is an essential contributor to neuronal differentiation has shown high pharmacological potential for the treatment of central neurodegenerative diseases such as Alzheimer and Parkinson. However, growth factors undergo rapid degradation, leading to a short biological half-life. In our study, we describe a new nano-based approach to enhance NGF activity resulting in promoted neuronal differentiation. We covalently conjugated NGF to iron oxide nanoparticles (NGF-NPs) and studied the effect of the novel complex on the differentiation of PC12 cells. We found that NGF-NPs treatment, at the same concentration as free NGF, significantly promoted neurite outgrowth and increased the complexity of the neuronal branching trees. Examination of neuronal differentiation gene markers demonstrated higher levels of expression in PC12 cells treated with the conjugated factor. By manipulating NGF specific receptor, TrkA, we demonstrated that NGF-NPs induce cell differentiation via the regular pathway. Importantly, we showed that NGF-NPs undergoe slower degradation than free NGF, extending its half-life and increasing NGF availability. Even low concentration of conjugated NGF treatment has led to an effective response. We propose the use of NGF-NPs complex which has magnetic characteristics, also as a useful method to enhance NGF efficiency and activity, thus, paving the way for substantial neuronal repair therapeutics.

Introduction

Nerve regeneration following tissue injury or disease is a major challenge for neuroscience. Regeneration represents the recapitulation of developmental processes striving to restore tissue integrity and functionality. Therefore, the search for regenerative agents that promote neuronal repair, growth and differentiation is of great interest. Growth factors are critical for the induction of cell differentiation. Enhancing the natural effect of growth factors during differentiation stages can lead to more efficient outcomes and the development of potential therapeutics.

Nerve growth factor (NGF), the first growth factor to be characterized,[1] is essential for the development and maintenance of neurons in the peripheral nervous system, as well as for the functional integrity of cholinergic neurons in the central nervous system.[2] NGF binds to its receptor TrkA at nerve terminals, is internalized in a receptor complex manner, and is retrograde transported through axons to the cell body.[3–5] There, in the cell body, it initiates intracellular signaling cascades that stimulate neural survival and differentiation.[6] NGF deficiency leads to brain disorders and pathologies.[7–10] Moreover, exogenous administration of NGF has protective properties for injured neurons and stimulates axonal regeneration.[11] NGF presents high pharmacological potential for the treatment of Alzheimer's and Parkinson's, with clinical trials currently in progress.[12–15]

One of the main challenges in the therapeutic use of NGF is its short half-life, due to rapid enzymatic degradation.[16–18] Previous studies have demonstrated that linking bioactive molecules to nanoparticles (NPs) influences the molecules' activity and stability.[19–24] An attractive class of NPs are iron oxide NPs that are beneficial for imaging and actuation using external magnetic fields.[25,26] They play an important role in biomedical applications such as bio-magnetic separation, cell-labeling and sorting, drug delivery, MRI contrast, and hyperthermia.[26–30] Exposure of nasal olfactory mucosa cells to the factor bFGF (basic fibroblast growth factor) conjugated to iron oxide NPs, has led to improved cell-proliferation properties.[22] Likewise, thrombin-conjugated NPs accelerated the healing of incisional wounds.[24]

Recently, the effect of iron oxide NPs combined with NGF has been studied. Micera and co-authors have developed iron oxide spheres loaded with NGF and demonstrated magnetic targeting and controlled release of the payload.[31] Park and co-authors have examined the effect of treatment with high concentrations of iron oxide NPs in addition to free NGF on neuronal growth. They have shown enhanced neurite outgrowth and increased cell adhesion.[32]

In this study, we suggest an approach to enhance the effect of NGF by covalently conjugating the factor to iron oxide NPs. We examined the influence of NGF-conjugated NPs (NGF-NPs) on the neuronal differentiation process. We used PC12 cells that recapitulate the last major steps of the neuronal differentiation process when exposed to free NGF *in vitro*.[33–36] We found that NGF-NPs induced typical PC12 differentiation, demonstrating a neuron-like growth, i.e., cells cease proliferation, extend branching neurites, and become electrically excitable. We compared the growth pattern and neuronal maturation of PC12 cells treated with NGF-NPs to that of those treated with free NGF and non-conjugated NPs. Based on morphometric and molecular measurements; we show that NGF-NPs treatment leads to a promoted differentiation progression even at low doses. Moreover, stability and signaling pathway assays suggest conjugation to NPs as a method to extend the half-life of NGF, thereby increasing its availability and efficiency. The ability to manipulate and enhance developmental processes and neuronal repair has great importance for potential therapeutics and tissue engineering.

Experimental Details

Cell culture

PC12 cells were grown in suspension in RPMI medium supplemented with 10% horse serum (HS), 5% fetal bovine serum (FBS), 1% L-glutamine, 1% penicillin-streptomycin and 0.2% amphotericin, in a humidified incubator at 37°C containing 5% CO_2 (medium and supplements were purchased from Biological Industries, Israel). To induce differentiation, cells were seeded on plates coated with collagen type l and incubated for 24 hours in serum reduced media (1% HS). Murine β-NGF (Peprotech, Israel) was then added to the medium as a free reagent or conjugated to iron oxide nanoparticles. Every two days, cells were rinsed with PBS, and fresh medium and NGF were added to the cells. Three NGF concentrations were examined; 50 ng/ml (free NGF: 1.86 nM; non-conjugeted NPs or NGF-NPs: 2.8×10^{-2} nM), 5 ng/ml (free NGF: 0.186 nM; non-conjugated NPs or NGF-NPs: 2.8×10^{-3} nM) and 250 ng/ml (free NGF: 9.3 nM; non-conjugated NPs or NGF-NPs: 13.95×10^{-2} nM).

Synthesis of NGF-conjugated iron oxide nanoparticles

Rhodamin-labeled iron oxide (R-γ-Fe_2O_3) NPs were synthesized according to previous publications.[22,37] NPs were then coated with human serum albumin (HSA) (Sigma, Israel) by precipitation of the protein onto the surface of the fluorescent iron oxide NPs. The NPs were then encapsulated by PEG terminated with NHS. The covalent conjugation of NGF to NPs was accomplished via the interaction of the amine and/or hydroxyl groups of the growth factor with the terminal activated NHS groups on the nanoparticle's surface. Briefly, 125 µL of a NGF-PBS solution (0.4 mg/mL, pH 7.4) was added to 125 µL of the PEG-activated NPs dispersed in bicarbonate buffer (9 mg/mL, pH 8.4) at a [NPs]/[NGF] weight ratio of 10. The reaction mixture of the PEG-activated NPs was then shaken at 4°C for 20 minutes. Blocking of the residual NHS was then accomplished by adding 1 % glycine (w/v) and then shaking for an additional hour. The obtained NGF-conjugated iron oxide nanoparticles were then washed from non-magnetic waste with PBS using the HGMF technique. The concentration of the NGF conjugated to the PEG-activated NPs (89 ± 3.1 µg/mg NPs) was determined by measuring the unbound NGF with a mouse IgG ELISA kit (Innovative Research, Israel) and subtracting it from the initial concentration. The reported values are an average of at least three measurements. The purity of the NGF was not damaged by the use of the HGMF process since the detection limit of the released NGF was the same as that of the free NGF.

The leakage of NGF, conjugated covalently to the PEG-activated NPs, was evaluated using the following procedure: NPs dispersed in PBS containing 4% HSA (2 mg/mL, pH 7.4) were shaken at room temperature for 24 h. Then, the NGF-conjugated NPs were removed from the supernatant using the HGMF technique and the concentration of NGF in the filtrate was measured by NGF ELISA kit.

Characterization of NGF-conjugated iron oxide nanoparticles

Low-resolution transmission electron microscopy (TEM) pictures were obtained with a FEI TECNAI C2 BIOTWIN electron microscope with 120 kV accelerating voltage. Samples for TEM were prepared by placing a drop of diluted sample on a 400-mesh carbon-coated copper grid. The average size and size distribution of the dry NPs were determined by measuring the diameter of more than 200 particles with the image analysis software AnalySIS Auto (Soft Imaging System GmbH, Germany). Hydrodynamic diameter and size distribution of the NPs dispersed in an aqueous phase were measured using a particle analyzer, model NANOPHOX (Sympatec GmbH, Germany). Fluorescence intensity and absorbance at room temperature were measured using a multiplate reader Synergy 4, using Gen 5 software.

Cell viability assay

The XTT assay was used for quantitative measurements of cell death. The assay is based on the ability of metabolic active cells to reduce tetrazolium salt XTT to orange colored compounds of formazan. The intensity of the dye is proportional to the number of metabolic active cells. 5×10^3 PC12 cells were seeded on collagen-coated 96-well plates (Greiner Bio-One, Germany). After 24 hours and 48 hours of NPs exposure, XTT reaction solution (Biological Industries, Israel) was added to the medium and incubated for 5 hours at 37°C. Absorbance was measured at 450nm (630nm background) by spectrophotometer (BioTek Synergy4, Vermont USA).

Imaging and morphometric analysis

Light microscope (Leica DMIL LED) was used to acquire phase images of cultured cells and networks for image processing analysis. Confocal imaging was performed using Leica TCS SP5 microscope with Acousto-Optical Beam Splitter. Images were acquired 1, 3 and 5 days after induction of differentiation. Morphometric parameters included neurite lengths, number of branching points and clustering behavior. We used NeuronJ, an ImageJ plugin (US National Institutes of Health, Bethesda, MD, USA), which enables semi-automatic tracing of neurites and length measurements.[38] Other parameters were measured manually. For each experiment, morphological parameters and statistics were measured for total of 540 cells - 60 cells per treatment (free NGF, non-conjugated NPs with free NGF and NGF-NPs) and per concentration (5, 50 and 250 ng/ml of NGF). Three batches of experiments (3×540 cells) were included.

Reverse transcription-polymerase chain reaction

RNA was extracted from PC12 cells using RNeasy kit (Qiagen, Germany), according to the manufacturer's instructions. Total RNA was reverse-transcribed to CDNA (Thermo scientific,

USA), using DreamTaq DNA polymerase (Thermo scientific, USA) and followed by PCR amplification. Total RNA and cDNA concentrations were measured using NanoDrop 2000c Spectrophotometer (Thermo Scientific, USA). Total RNA and cDNA concentrations, respectively: free NGF: 85 ng/µl and 1300 ng/µl; non-conjugated NPs + free NGF: 91 ng/µl and 1600 ng/µl; NGF-NPs: : 95 ng/µl and 1300 ng/µl. Sample volumes were loaded to obtain similar amount of cDNA template. The following primers were used for PCR: β-actin (165 bp): forward 5'- TGTCACCAACTGGGACGATA-3', reverse 5'-GGGGTGTTGAAGGTCTCAAA-3'; β3-tubulin (266 bp): forward 5'-TCTACGACATCTGCTTCCGC-3', reverse 5'-GTCGAACATCTGCTGGGTGA-3' (30 PCR cycles). GAP43 (206 bp): forward 5'-CAGGAAAGATCCCAAGTCCA-3', reverse 5'-GAACGGAACATTGCACACAC-3' (40 PCR cycles); The PCR products were electrophoresed on a 3% agarose gel.

High resolution scanning electron microscopy

To closely examine PC12 cells at the differentiation process, cells were imaged by a high resolution scanning electron microscope (HR-SEM). $4x10^4$ cells were plated on 13 mm collagen-coated plastic coverslips (NUNC Thermanox, NY USA). Three days after induction of differentiation, cells were fixed using 2.5% gluteraldehyde/2.5% formaldehyde in 0.1M sodium cacodylate buffer, for 1h at room temperature. After fixation, cultures were repeatedly rinsed with PBS (no Ca^{3+}, no Mg^{3+}, pH 7.2) and then treated with Guanidine-HCl:Tannic acid (4:5) solution (2%) for 1 hour at room temperature. After repeatedly rinsing again with PBS, cells were dehydrated in graded series of ethanol (50, 70, 80, 90 and 100%) and then with graded series of Freon (50, 75, 100% × 3). Finally, the preparations were sputtered with iridium before examination by HR-SEM (Magellan 400L, FEI, Hillsboro, OR, USA).

TrkA inhibitor treatment

PC12 cells were seeded on collagen-coated plates and incubated for 24 hours. Cells were then treated with 500 nM TrkA inhibitor GW441756 (Tocris Bioscience, Bristol, UK) for 30 min in 37°C. Then, NGF (as a free factor or conjugated to nanoparticles) was added to the cells, and incubated for another 24 h.

NGF stability test

To measure NGFs' degradation rate, free NGF and NGF-NPs were incubated in 70% unheated proteases enriched serum in PBS at 37°C for 7 days. Samples were taken on days 0, 1 and 7. Then, NGF concentration was measured using NGF ELISA kit (Chemicon-Millipore, MA, USA) according to manufacture protocol: Samples were placed in a 96-well plate and incubated overnight at 4°C. Wells were rinsed repeatedly with wash buffer and incubated with anti-mouse NGF monoclonal antibody for 2 hours on shaker. The wells were rinsed with wash buffer and incubated for 2 hours on shaker with donkey anti-mouse IgG polyclonal antibody, conjugated to horseradish peroxidase (HRP). Then, tetramethylbenzidine (TMB) substrate solution was added to the wells. Stop solution was added after 5 minutes to stop the reaction and the plate was immediately read at 450nm by spectrophotometer.

Western blot

$8×10^4$ PC12 cells were plated on 35-mm collagen-coated plates and incubated overnight at 37°C. Cells were then incubated with NGF (1.86 nM = 50 ng/ml) or NGF-NPs ($2.8×10^{-2}$ nM) at 37°C for 1, 5, 15, and 30 min. Cells were collected in 200 µl lysis buffer (50 mM Tris [pH 8], 150 mM NaCl, 1% Triton 0.5% sodium deoxycholate, 0.1% SDS, 20 mM beta-glycerophosphate, 1 mM Na_3VO_4 and protease inhibitor cocktail (Sigma, St. Louis, MO): 2 mM AEBSF, 14 µM E-64, 130 µM bestatin, 0.9 µM leupeptin, 0.3 µM aprotinin and 1mM EDTA), and then lysed for 30 min on ice. After centrifuging at 12,000 RPM for 20 min, the supernatant was removed and assayed for protein by the Bradford procedure (Bio-Rad, Germany) using bovine serum albumin (Biological Industries, Israel) as standard. SDS-PAGE 4x sample buffer (277.8 mM Tris-HCl [pH 6.8], 44.4% glycerol, 4.4% SDS, 0.002% bromophenol blue and 10% β-mercaptoethanol) was added, and the sample was heated to 75°C for 5 min. Equal amounts of protein (150µg) were loaded onto 8% SDS-PAGE. Protein bands were transferred to a nitrocellulose membrane (Bio-Rad, CA) and probed with anti-phospho-TrkA (Tyr490) or anti-TrkA antibody (9141S and 2508S, Cell Signaling Technology, MA) (at 1:1000). HRP-conjugated secondary antibody (7074S, Cell Signaling Technology, MA) (at 1:1000) was used for protein band detection. Cross reactivity was visualized by the enhanced chemoluminescence (ECL) procedure (Pierce).

Results

Synthesis and characterization of NGF-NPs

Uniform fluorescent iron oxide (R-γ-Fe_2O_3) NPs were synthesized by nucleation, followed by controlled growth of γ-Fe_2O_3 thin films onto gelatin-RITC-iron oxide nuclei (RITC i.e. Rhodamine Isothiocyanate).[24] As illustrated in Fig. 1A, fluorescent NPs were coated with HSA via a precipitation s

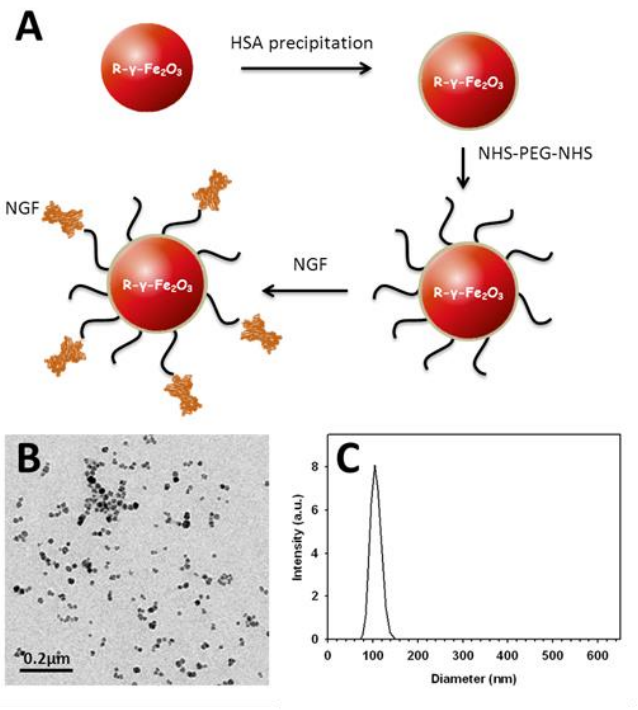

Fig. 1 (A) Schematic illustration of NGF-NPs synthesis. (B) TEM image of NGF-NPs. (C) Size histogram of NGF-NPs hydrodynamic diameter.

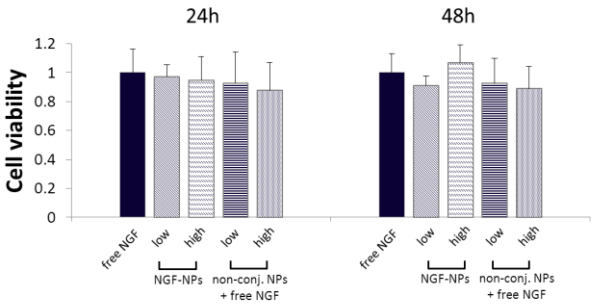

Fig. 2 XTT viability assay of PC12 cells treated with NGF-NPs and non-conjugated NPs (n=3). Absorbance at 450nm (630nm background). Measurements were normalized to control ('free NGF').

process.[22,24] Then, a spacer arm of polyethylene glycol (PEG) terminated with N-hydroxysuccinimide (NHS) was covalently conjugated to the R-γ-Fe_2O_3 NPs via the primary amine groupof the HSA coating. The NGF was conjugated covalently onto the surface: terminal activated NHS groups of the PEG interacted with primary amino groups of NGF. To evaluate NGF leakage, i.e. release of free NGF from NPs, the NGF-NPs were dispersed in phosphate-buffered saline (PBS) containing 4% HSA. Then, NPs were removed and free NGF concentration was measured by ELISA. No NGF was detected, indicating no leakage of NGF from the NGF-NP complex (data not shown).

The size of the NGF-NPs was measured using TEM, demonstrating a diameter of 23.0 ± 2.1 nm (Fig. 1B and Experimental Section). The hydrodynamic diameter of the NGF-NPs dispersed in the aqueous continuous phase, as determined by the light scattering technique, was 104 ± 12 nm (Fig.1C). The conjugation ratio between NGF and the NPs (the number of NGF molecules attached to a single NP) was estimated as 70 (67 ± 18) (†ESI).

Cytotoxicity examination

The viability of PC12 cells following iron oxide NP treatment was tested. The effect of NGF-NPs and non-conjugated NPs on PC12 cells was examined using an XTT assay. Cells were incubated with NGF-NPs at an NP concentration of 0.6μg/ml, a concentration equivalent to 50 ng/ml of free NGF which is a typical concentration for PC12 differentiation. Cells were also incubated with a higher concentration of NGF-NPs (20 μg/ml). Cell viability experiments were performed at time points 24h and 48h after exposure to non-conjugated NPs and NGF-NPs. The experiment depicted no evident cell damage following NP treatment. Increasing NP doses did not affect cell viability (Fig. 2 and Fig. S1, †ESI). No significant difference in cell viability was observed for all preparations, indicating that NGF-NPs have no cytotoxic effect on PC12 cells.

The effect of NGF-NPs on neuronal differentiation

Morphological effects. The effect of NGF-NPs on neuronal differentiation was studied by examining the morphology of PC12 cells. First, the effectiveness of NGF-NPs as a differentiating factor was tested. It can be seen that PC12 cells treated with NGF-NPs demonstrated neurite outgrowth and

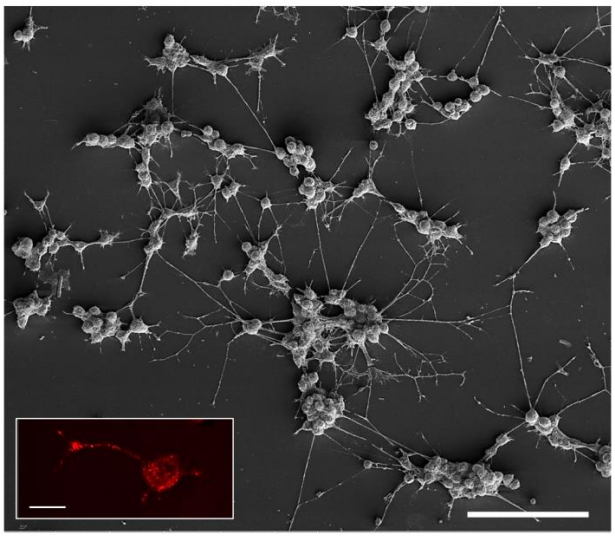

Fig. 3 SEM image of PC12 cells three days after induction of differentiation by NGF-NPs. Scale bar = 100μm. Inset: Fluorescence confocal microscopy image (a single focal plane) illustrating the internalization of NGF-NPs into PC12 cells. NPs are rhodamin labeled (red). Scale bar = 10μm.

formation of a complex neuronal network (Fig. 3), indicating that NGF remained active. Fluorescent confocal microscopy imaging revealed the internalization of NPs into the cells with high accumulation at branching points (Fig. 3, inset). Then, NGF-NPs treatment was compared to the common free NGF treatment as well as to exposure to non-conjugated NPs with free NGF. The PC12 cells were plated on collagen coated plates and treated with the three NGF combinations, at the same NGF concentrations.

Morphological differentiation properties at the single cell level were measured. Populations of cells were analyzed between one day and five days after differentiation induction. Three NGF concentrations were examined for all treatments; 50 ng/ml (common dosage), low concentration of 5 ng/ml and a high concentration of 250 ng/ml.

Results shown in Fig. 4 demonstrate a clear morphological effect on the neuronal differentiation process when treated with the conjugated factor. A day after treatment cells treated with NGF-NPs show a significant increase in total neurite length per cell. For NGF-NPs at an NGF concentration of 50 ng/ml, the neurites show an average total length of 112 ± 15 μm, whereas free NGF treatment led to an average total length of only 53 ± 7 μm. The enhancement of total neurite length following NGF-NPs treatment was more pronounced at the lower NGF concentrations: at 5 ng/ml the average total length of cells treated with NGF-NPs was almost three times higher than for cells treated with free NGF (83 ± 13 μm vs. 31 ± 4 μm). Moreover, when comparing the effect of low concentration of conjugated NGF (5 ng/ml) to the commonly used concentration of free NGF (50 ng/ml), the former showed longer total neurite length.

Treatment with non-conjugated NPs together with free NGF demonstrated a slight enhancement in the total neurite lengths in comparison to those treated with free NGF (Fig. 4A).

An additional parameter, the average number of branching points per cell, was measured a day after plating (Fig. 4B). The same trend was observed: cells following NGF-NPs treatment developed more branching points in comparison to those

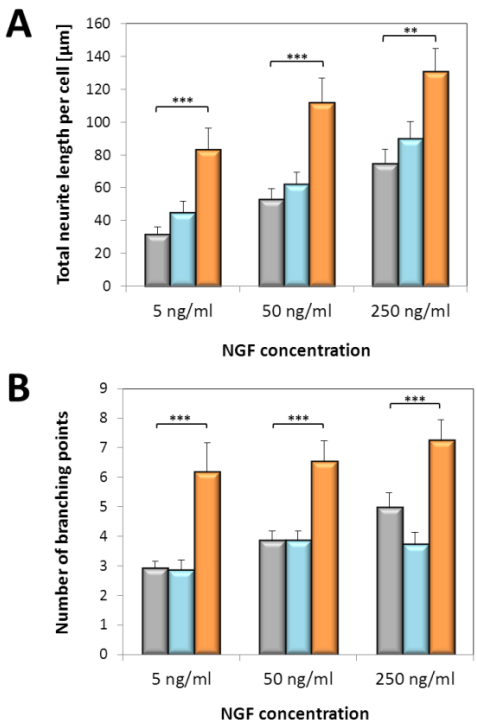

Fig. 4 Effect of NGF-NPs on morphological parameters of neuronal differentiation at different NGF concentrations, comparing between the three treatments: free NGF (grey), non-conjugated NPs with free NGF (light blue) and NGF-NPs (orange). (A) Total neurite length per cell. (B) Number of branching points. ANOVA test, ** $p < 0.01$ and *** $p < 0.001$

following free NGF treatment and non-conjugated NPs together with free NGF treatment, leading to more complex branching trees for all concentrations. For example, cells treated with NGF at a concentration of 50 ng/ml had averages of 6.5 ± 0.7, 3.8 ± 0.3 and 3.8 ± 0.4 branching points, respectively.

To further analyze the effect of NGF-NPs on cell differentiation, neurites were classified to short, medium and long (neurite lengths smaller than one cell diameter are considered 'short', 'medium' refers to neurite lengths between one to two cell diameters, while 'long' refers to lengths longer than two cell body diameters). Fig. 5 presents the distribution of neurites for the three concentrations. It can be seen that cells treated with NGF-NPs showed a higher percentage of medium and long neurites than those treated with free NGF. Cells treated with non-conjugated NPs and free NGF showed similar

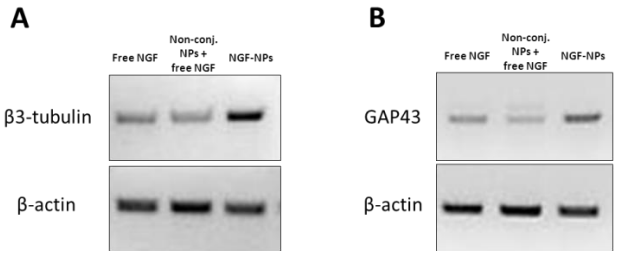

Fig. 6 Effect of NGF-NPs on neuronal differentiation genes. PCR for mRNA levels of β3-tubulin (A, upper panel) and GAP43 (B, upper panel) of differentiated PC12 cells treated with free NGF, non-conjugated NPs with free NGF and NGF-NPs. Lower panels present a control PCR of β-actin of the same samples. Data was obtained one day after treatment.

distribution of neurites for the higher doses whereas for the 5 ng/ml longer neurites were detected for cells treated with the NPs in addition to the free NGF.

Remarkably, examination of the morphological effects at several time points after treatment with free NGF and NGF-NPs, revealed the strongest effect after only one day of treatment. By day three, no significant difference was observed between treatments (data not shown).

Molecular effects. The effect of NGF-NPs at the molecular level was examined. The levels of expression of genes related to neuronal differentiation, GAP43 and β3-tubulin, were studied. RNA was extracted from cells treated with NGF-NPs and compared to free NGF as well as non-conjugated NPs with free NGF treatments. PCR experiments revealed an elevated level of expression of GAP43 and β3-tubulin genes in cell populations treated with the NGF-NP complex, in comparison to the other two conditions (Fig. 6 and Fig. S2, †ESI). As a loading control, the level of expression of β-actin was examined. Fig. 6 demonstrates no difference in levels of expression of β-actin for the three treated populations.

The role of TrkA in NGF-NP complex activity

Involvement of TrkA pathway in mediating PC12 differentiation following NGF-NPs treatment was examined. GW441756, a TrkA inhibitor that prevents NGF from binding to TrkA receptor, was used prior to NGF treatment. Cells were examined 24h following inhibitor exposure. No neurites were developed, either with free NGF or with NGF-NPs treatment (Fig. 7A, upper images). As expected, cells treated with NGF with no inhibitor, demonstrated neurite extension (Fig. 7A,

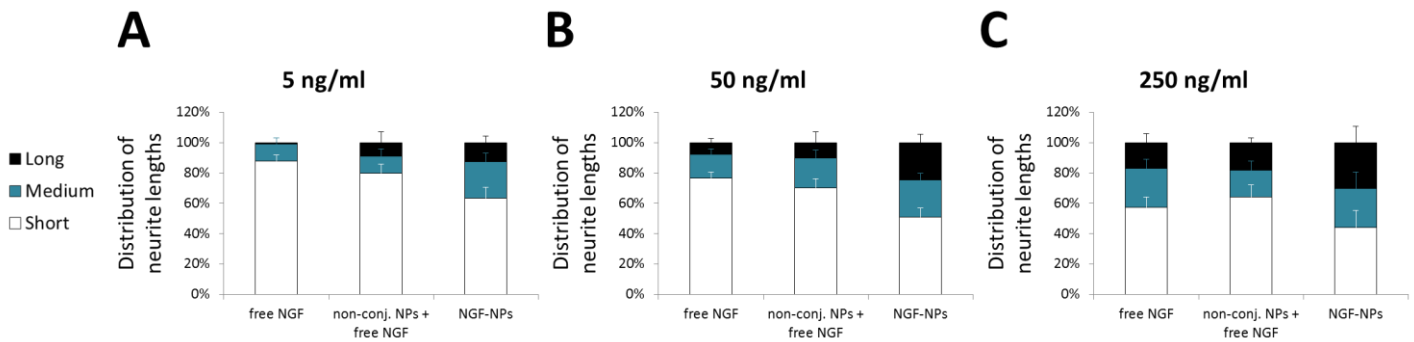

Fig. 5 Distribution of neurite lengths for free NGF vs. non-conjugated NPs and free NGF and vs. NGF-NPs, at NGF concentration of (A) 5 ng/ml (B) 50 ng/ml and (C) 250 ng/ml. 'Short' refers to neurites shorter than one cell body diameter. 'Medium' refers to neurites between one to two cell body diameters. 'Long' refers to neurites longer than two cell body diameters.

lower images). No neurite outgrowth was observed even two days after inhibition treatment (Fig. S3, †ESI). Interestingly, fluorescent imaging of the treated cells shows that following TrkA inhibition, NGF-NPs are internalized into the cells but fail to induce differentiation and neurite outgrowth (Fig. 7B).
Next, to further examine the bioactivity of NGF-NPs, Western blot analysis of phosphorylated TrkA (pTrkA) was performed. PC12 cells were incubated in serum free medium with NGF-NPs for 1, 5, 15 and 30 min before cell lysis and Western blot analysis. Figure 8 confirms the activation of pTrkA by the NGF-NP complex. The maximal level of pTrkA was detected after 5 min of incubation. A Western blot analysis of PC12 cells treated with free NGF demonstrates similar levels of phosphorylation of TrkA, reaching the peak level after 15 min of incubation. As a control, Western blot analysis was performed for total TrkA for both conditions. β-actin was examined for both conditions serving as a loading control.

Stability of NGF-NP complex in comparison to free NGF

The effect of NGF conjugation to iron oxide NPs on NGF degradation rate, thus stability, was examined. Free NGF and NGF-NPs were incubated at the same initial concentrations, in protease enriched serum for seven days. ELISA was carried out to measure NGF concentrations. Fig. 9 shows a decrease in the concentration of free NGF, with no NGF detected by day seven. In sharp contrast, no significant change was observed in the concentration of NGF-NPs throughout the seven days. The constant concentration throughout the experiment indicates that

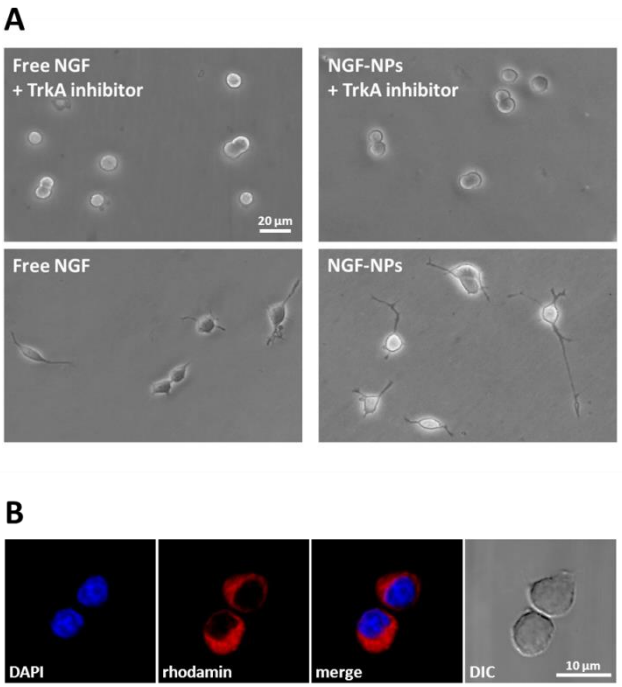

Fig. 7 (A) PC12 cells 1 day after NGF or NGF-NPs treatments following TrkA manipulation. Upper images: cells treated with TrkA inhibitor prior to NGF treatments. Lower images: cells with no TrkA inhibitor treatment. Scale Bar = 20 µm. (B) PC12 cells 1 day after NGF-NPs treatment following TrkA inhibition. NGF-NPs labeled with rhodamin (red) enter the cells. Nuclei marked with DAPI (blue). The fluorescent images were acquired using a confocal microscopy at a single focal plane. Right image: DIC image of the same labeled cells. Scale Bar = 10 µm.

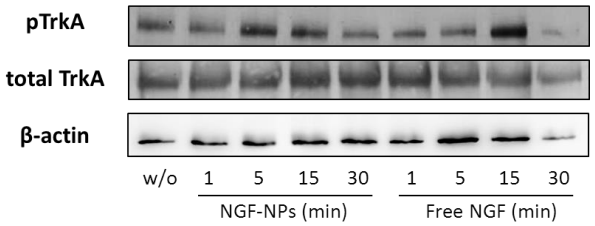

Fig. 8 Western blot analysis of phosphorylated TrkA (p-TrkA at Tyr490) and total TrkA. PC12 cells were incubated for the indicated times (1, 5, 15, 30 minutes) with NGF-NPs or free NGF. Protein samples were analysed by Western blotting using anti-pTrkA and anti-TrkA. β-actin served as a loading control.

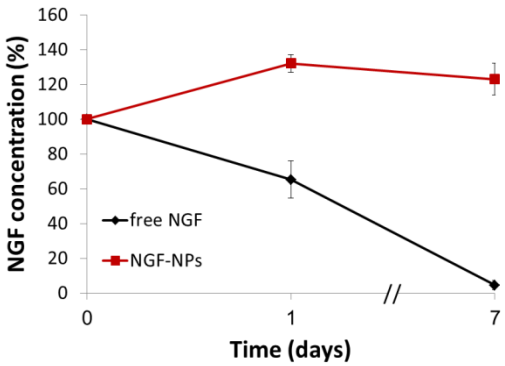

Fig. 9 ELISA analysis of NGF degradation rate, free NGF vs. NGF-NPs. (n=3).

NGF conjugated to NPs undergoes slower degradation than free NGF, extending the half-life of NGF.

Discussion

NGF induces neuronal differentiation and survival processes and has high potential for the treatment of central neurodegenerative diseases. However, growth factors have limited effectiveness when applied externally due to a short biological half-life and rapid degradation *in vivo*.[6,15,16] Here, we described an approach for increasing the stability and availability of NGF using NPs. We examined a method to enhance the activity of NGF for neuronal differentiation by conjugating the factor to iron oxide NPs. PC12 cells served as a model for neuronal differentiation. We synthesized NPs covalently conjugated to NGF, and found that the complex promotes differentiation. The effect of NGF-NPs was compared to that of free NGF at the same concentration, demonstrating that NGF-NPs treatment leads to longer neurites and more branching points. Moreover, NGF-NPs treatment leads to higher expression levels of neuronal differentiation gene markers.
Previous studies have demonstrated an effect on PC12 survival and neurite outgrowth by adding high concentrations of iron ions[39] and by adding non-conjugated iron oxide NPs to the NGF-induced reaction.[12] In our experiments, we studied the effect of the conjugation of NGF on the reaction. Remarkly, a comparison between treatment of NGF-conjugated NPs to a treatment with non-conjugated NPs and free NGF, at the same NPs concentrations (significantly lower than the iron-based

treatments described above), showed an enhanced effect for the conjugated NGF.

In order to elucidate the advantage of conjugating NGF to the NPs, the stability of NGF as a conjugated complex was tested. We found that NGF conjugated to NPs, undergoes slower degradation than free NGF. Thus, we conclude that the spatial structure of the NGF-conjugated NP complex, prevents protease enzymes from binding to their active sites, hence prolongs NGF half-life and improves its efficiency. Furthermore, each NP is linked to several NGF molecules. The multiple linking sites taken together with the slower enzymatic activity, point toward higher local availability of NGF.

Internalization of NGF-TrkA ligand-receptor complex is known to initiate differentiation processes within cells.[6] To examine the signaling pathway through which the NGF-conjugated NP complex acts, we modified the activity of TrkA. We blocked the receptor TrkA that initiates the differentiation pathway. Our results showed that NGF-NPs induce cell differentiation via the regular pathway of TrkA receptor. Although entry of NGF to the cell can be mediated by NPs, evading the TrkA pathway, NGF binding to TrkA receptor is essential for the induction of the differentiation process. Moreover, Western blot analysis of pTrkA proves that NGF-NP complex induces receptor phosphorylation. We showed that linking the factor to NPs still enables NGF to function and interact effectively with TrkA receptor.

In parallel to evaluating NGF-NP complex activity, we have examined the toxicity of the NP-based complex. While cytotoxic effects of iron oxide NPs have been previously reported at high NP doses,[7,40,41] our cell viability assays showed that at the concentrations measured, NGF-NPs have no cytotoxic effect on PC12 cells. Due to the high binding yield of NGF to the NPs, and the stability of the complex, a very low NP concentration is required to obtain optimal differentiation promotion. We have shown that low NGF concentration (10 times less than the common concentration for an effective process) is sufficient for the induction of enhanced differentiation. We conclude that the conjugation of NGF to NPs enables a significant reduction of NP doses, thus inducing less toxic effects and requiring lower therapeutic load.

It is important to note that combining NGF with nano-based systems may overcome other challenges related to therapeutic use of NGF. For example, NP-based delivery has the potential to transport factors across the BBB, which is an obstacle in nerve tissue repair.[18,19] In addition, NPs can be used for increasing specificity, avoiding adverse effects on non-target cells.[21] Moreover, the magnetic properties of iron oxide NPs may be utilized for targeting a desired site by external magnetic field, for a more localized and efficient treatment.[26,27]

It has been demonstrated that the presence of iron oxide NPs in lysosomes of PC12 cells indicates the ability of cells to vacate the particles.[32] This evidence is critical when using nano-size elements, to prevent accumulation of NPs as a foreign body in the cell, which may lead to unwanted, uncontrollable response.

Conclusions

To summarize, we have shown that linking NGF to iron oxide NPs increases NGF function for inducing promoted neuronal differentiation. Therefore, this approach may serve as an efficient method for growth factor delivery, and contribute to the development of novel therapeutics to promote neuronal regeneration and repair.

Acknowledgements

The authors thank Dr. Enav Corem for the invaluable help with the ELISA experiments. The authors thank Shaul Barth and Neta Zilony for the help with the western blot assay. The authors thank Pazit Polak for careful and critical reading of the manuscript. M.M. gratefully acknowledges the BINA Scholarship for Outstanding Graduate Students.

Notes and references

[a] Faculty of Engineering, Bar Ilan University, Ramat Gan 5290002 Israel. E-mail: orit.shefi@biu.ac.il. Tel:+972 3 531-7079

[b] Depatment of Chemistry, Bar Ilan University, Ramat Gan 5290002 Israel

[c] Bar Ilan Institute of Nanotechnologies and Advanced Materials, Ramat Gan 5290002 Israel

†Electronic Supplementary Information (ESI) available: [Conjugation ratio determination and supplementary figures] See DOI: 10.1039/b000000x/

1. R. Levi-Montalcini, *Science*, 1987, **237**, 1154–62.

2. C. Wiesmann and A. M. de Vos, *Cell. Mol. Life Sci.*, 2001, **58**, 748–59.

3. E. J. Huang and L. F. Reichardt, *Annu. Rev. Neurosci.*, 2001, **24**, 677–736.

4. B. Cui, C. Wu, L. Chen, A. Ramirez, E. L. Bearer, W.-P. Li, W. C. Mobley, and S. Chu, *Proc. Natl. Acad. Sci. U. S. A.*, 2007, **104**, 13666–71.

5. M. A. Palmatier, B. K. Hartman, and E. M. Johnson, *J. Neurosci.*, 1984, **4**, 751–6.

6. Y. Zhang, D. B. Moheban, B. R. Conway, A. Bhattacharyya, and R. A. Segal, *J. Neurosci.*, 2000, **20**, 5671–8.

7. F. Hefti, J. Hartikka, and B. Knusel, *Neurobiol. Aging*, 1989, **10**, 515–33.

8. S. H. Appel, *Ann. Neurol.*, 1981, **10**, 499–505.

9. C. Crowley, S. D. Spencer, M. C. Nishimura, K. S. Chen, S. Pitts-Meek, M. P. Armanini, L. H. Ling, S. B. McMahon, D. L. Shelton, and A. D. Levinson, *Cell*, 1994, **76**, 1001–11.

10. R. J. Smeyne, R. Klein, A. Schnapp, L. K. Long, S. Bryant, A. Lewin, S. A. Lira, and M. Barbacid, *Nature*, 1994, **368**, 246–9.

11. M. G. Lykissas, A. K. Batistatou, K. A. Charalabopoulos, and A. E. Beris, *Curr. Neurovasc. Res.*, 2007, **4**, 143–51.

12. S. J. Allen, J. J. Watson, D. K. Shoemark, N. U. Barua, and N. K. Patel, *Pharmacol. Ther.*, 2013, **138**, 155–75.

13. L. Aloe, M. L. Rocco, P. Bianchi, and L. Manni, *J. Transl. Med.*, 2012, **10**, 239.

14. M. Eriksdotter Jönhagen, A. Nordberg, K. Amberla, L. Bäckman, T. Ebendal, B. Meyerson, L. Olson, Seiger, M. Shigeta, E. Theodorsson, M. Viitanen, B. Winblad, and L. O. Wahlund, *Dement. Geriatr. Cogn. Disord.*, **9**, 246–57.

15. M. H. Tuszynski, L. Thal, M. Pay, D. P. Salmon, H. S. U, R. Bakay, P. Patel, A. Blesch, H. L. Vahlsing, G. Ho, G. Tong, S. G. Potkin, J. Fallon, L. Hansen, E. J. Mufson, J. H. Kordower, C. Gall, and J. Conner, *Nat. Med.*, 2005, **11**, 551–5.

16. M. A. Tria, M. Fusco, G. Vantini, and R. Mariot, *Exp. Neurol.*, 1994, **127**, 178–83.

17. K. Lee, E. A. Silva, and D. J. Mooney, *J. R. Soc. Interface*, 2011, **8**, 153–70.

18. E. Anitua, M. Sánchez, G. Orive, and I. Andia, *Trends Pharmacol. Sci.*, 2008, **29**, 37–41.

19. S. Barber, M. Abdelhakiem, K. Ghosh, L. Mitchell, R. Spidle, B. Jacobs, L. Washington, J. Li, A. Wanekaya, G. Glaspell, and R. K. DeLong, *J. Nanosci. Nanotechnol.*, 2011, **11**, 10309–19.

20. A. E. Garcia-Bennett, M. Kozhevnikova, N. König, C. Zhou, R. Leao, T. Knöpfel, S. Pankratova, C. Trolle, V. Berezin, E. Bock, H. Aldskogius, and E. N. Kozlova, *Stem Cells Transl. Med.*, 2013, **2**, 906–15.

21. H. Hinterwirth, W. Lindner, and M. Lämmerhofer, *Anal. Chim. Acta*, 2012, **733**, 90–7.

22. H. Skaat, O. Ziv-Polat, A. Shahar, and S. Margel, *Bioconjug. Chem.*, 2011, **22**, 2600–10.

23. Z. Wu, B. Zhang, and B. Yan, *Int. J. Mol. Sci.*, 2009, **10**, 4198–209.

24. O. Ziv-Polat, M. Topaz, T. Brosh, and S. Margel, *Biomaterials*, 2010, **31**, 741–7.

25. A. Solanki, J. D. Kim, and K.-B. Lee, *Nanomedicine (Lond).*, 2008, **3**, 567–78.

26. N. Tran and T. J. Webster, *J. Mater. Chem.*, 2010, **20**, 8760–8767.

27. C. Kilgus, A. Heidsieck, A. Ottersbach, W. Roell, C. Trueck, B. K. Fleischmann, B. Gleich, and P. Sasse, *Pharm. Res.*, 2012, **29**, 1380–91.

28. P. Dames, B. Gleich, A. Flemmer, K. Hajek, N. Seidl, F. Wiekhorst, D. Eberbeck, I. Bittmann, C. Bergemann, T. Weyh, L. Trahms, J. Rosenecker, and C. Rudolph, *Nat. Nanotechnol.*, 2007, **2**, 495–9.

29. B. Perlstein, Z. Ram, D. Daniels, A. Ocherashvilli, Y. Roth, S. Margel, and Y. Mardor, *Neuro. Oncol.*, 2008, **10**, 153–61.

30. I. J. M. de Vries, W. J. Lesterhuis, J. O. Barentsz, P. Verdijk, J. H. van Krieken, O. C. Boerman, W. J. G. Oyen, J. J. Bonenkamp, J. B. Boezeman, G. J. Adema, J. W. M. Bulte, T. W. J. Scheenen, C. J. A. Punt, A. Heerschap, and C. G. Figdor, *Nat. Biotechnol.*, 2005, **23**, 1407–13.

31. G. Ciofani, V. Raffa, A. Menciassi, A. Cuschieri, and S. Micera, *Biomed. Microdevices*, 2009, **11**, 517–27.

32. J. A. Kim, N. Lee, B. H. Kim, W. J. Rhee, S. Yoon, T. Hyeon, and T. H. Park, *Biomaterials*, 2011, **32**, 2871–7.

33. L. A. Greene and A. S. Tischler, *Proc. Natl. Acad. Sci. U. S. A.*, 1976, **73**, 2424–8.

34. M. A. Dichter, A. S. Tischler, and L. A. Greene, *Nature*, 1977, **268**, 501–4.

35. J. D. Pollock, M. Krempin, and B. Rudy, *J. Neurosci.*, 1990, **10**, 2626–37.

36. B. Rudy, B. Kirschenbaum, A. Rukenstein, and L. A. Greene, *J. Neurosci.*, 1987, **7**, 1613–25.

37. S. Margel and S. Gura, 2006, Israel Patent No. WO9962079.

38. E. Meijering, M. Jacob, J.-C. F. Sarria, P. Steiner, H. Hirling, and M. Unser, *Cytometry. A*, 2004, **58**, 167–76.

39. J. Hong, K. Noh, Y. Yoo, S. Choi, S. Park, Y. Kim, and J. Chung, *Mol. Cells*, 2003, **15**, 10–9.

40. T. R. Pisanic, J. D. Blackwell, V. I. Shubayev, R. R. Fiñones, and S. Jin, *Biomaterials*, 2007, **28**, 2572–81.

41. M. Mahmoudi, H. Hofmann, B. Rothen-Rutishauser, and A. Petri-Fink, *Chem. Rev.*, 2012, **112**, 2323–38.

